A single-column model intercomparison of a heavily drizzling stratocumulus-topped boundary layer

Matthew C. Wyant,[1] Christopher S. Bretherton,[1] Andreas Chlond,[2] Brian M. Griffin,[3] Hiroto Kitagawa,[4] Cara-Lyn Lappen,[5] Vincent E. Larson,[3] Adrian Lock,[6] Sungsu Park,[1] Stephan R. de Roode,[7] Junya Uchida,[8] Ming Zhao,[9] and Andrew S. Ackerman[10]

Received 12 February 2007; revised 11 July 2007; accepted 2 August 2007; published 27 December 2007.

[1] This study presents an intercomparison of single-column model simulations of a nocturnal heavily drizzling marine stratocumulus-topped boundary layer. Initial conditions and forcings are based on nocturnal flight observations off the coast of California during the DYCOMS-II field experiment. Differences in turbulent and microphysical parameterizations between models were isolated by slightly idealizing and standardizing the specification of surface and radiative fluxes. For most participating models, the case was run at both typical operational vertical resolution of about 100 m and also at high vertical resolution of about 10 m. As in prior stratocumulus intercomparisons, the simulations quickly develop considerable scatter in liquid water path (LWP) between models. However, the simulated dependence of cloud base drizzle fluxes on LWP in most models is broadly consistent with recent observations. Sensitivity tests with drizzle turned off show that drizzle substantially decreases LWP for many models. The sensitivity of entrainment rate to drizzle is more muted. Simulated LWP and entrainment are also sensitive to the inclusion of cloud droplet sedimentation. Many models underestimate the fraction of drizzle that evaporates below cloud base, which may distort the simulated feedbacks of drizzle on turbulence, entrainment, and LWP.

Citation: Wyant, M. C., et al. (2007), A single-column model intercomparison of a heavily drizzling stratocumulus-topped boundary layer, *J. Geophys. Res.*, *112*, D24204, doi:10.1029/2007JD008536.

1. Introduction

[2] Marine stratocumulus-topped boundary layers have been extensively studied because of their broad geographical coverage and their correspondingly large impact on climate. Realistically representing stratocumulus boundary layers in general circulation models (GCMs) and weather forecast models continues to be a significant challenge. Despite steady improvements in the resolution of such models, they continue to require parameterizations of cloud processes in the marine boundary layer (MBL). Single-column models (SCMs) provide a useful framework to test and improve these parameterizations.

[3] This study describes the latest of a series of intercomparisons performed by the Global Energy and Water Cycle Experiment Cloud System Study (GCSS) Boundary Layer Cloud Working Group (BLCWG), involving both SCMs and large-eddy simulations (LESs). An idealized case of nonprecipitating nocturnal marine stratocumulus was the focus of the first such intercomparison. It showed large model-to-model variations between cloud thickness and entrainment rate (a major control on cloud thickness and MBL structure) in both LES [*Moeng et al.*, 1996] and SCM [*Bechtold et al.*, 1996], illustrating the modeling challenges also present in global simulations. Ambiguities in the case specification and lack of a good observational comparison hindered the analysis. Thus the BLCWG recently returned to a much better observed nonprecipitating nocturnal marine stratocumulus case from July of 2001 off the California coast; the Dynamics and Chemistry of Marine Stratocumulus Experiment (DYCOMS-II [*Stevens et al.*, 2003]) Research Flight RF01. Companion LES and SCM intercomparisons based on this case were presented by *Stevens et al.* [2005] and *Zhu et al.* [2005, hereinafter referred to as Z05]. For both SCMs and LESs, the intermodel spread of entrainment rates was much reduced, but despite improved vertical resolution and updated model physics, liquid water path still differed by an order of magnitude between models after as little as an

[1]Department of Atmospheric Sciences, University of Washington, Seattle, Washington, USA.
[2]Max Planck Institute for Meteorology, Hamburg, Germany.
[3]Department of Mathematical Sciences, University of Wisconsin-Milwaukee, Milwaukee, Wisconsin, USA.
[4]Japan Meteorological Agency, Tokyo, Japan.
[5]Department of Atmospheric Science, Colorado State University, Fort Collins, Colorado, USA.
[6]Met Office, Exeter, UK.
[7]Koninklijk Nederlands Meteorologisch Instituut, De Bilt, Netherlands.
[8]Department of Applied Mathematics, University of Washington, Seattle, Washington, USA.
[9]NOAA Geophysical Fluid Dynamics Laboratory, Princeton, New Jersey, USA.
[10]NASA Goddard Institute for Space Studies, New York, New York, USA.

Copyright 2007 by the American Geophysical Union.
0148-0227/07/2007JD008536

hour of simulation. A similar result was found in a EUROCS intercomparison of coastal stratocumulus [*Duynkerke et al.*, 2004].

[4] Meanwhile, the importance of drizzle in stratocumulus-topped MBLs became more apparent, due in part to interest in the aerosol indirect effect on climate. A variety of field studies documented stratocumulus drizzle, culminating in extensive and complementary sets of measurement from DYCOMS-II [*Stevens et al.*, 2003; *vanZanten et al.*, 2005] and the East Pacific Investigation of Climate (EPIC [*Bretherton et al.*, 2004b]). Many leading GCMs used for assessing anthropogenic climate change are currently developing representations of aerosol indirect effects.

[5] Motivated by these considerations, this paper presents SCM results from a GCSS BLCWG intercomparison study of drizzling nocturnal stratocumulus clouds. The case is slightly idealized from aircraft observations from DYCOMS-II research flight RF02 [*vanZanten et al.*, 2005], which sampled stratocumulus with heavy drizzle (the surface mean drizzle rate was 0.35 mm d^{-1}) and substantial horizontal inhomogeneity. Unlike in RF01, drizzle plays a significant role in RF02 boundary layer thermodynamics. A. Ackerman et al. (manuscript in preparation, 2007, hereinafter referred to as A07), present a companion LES intercomparison experiment performed using identical specifications.

[6] We first examine the case setup and describe the models and their physical parameterizations. We next compare the standard and high-resolution cases separately. We then focus on the precipitation processes in the simulations as well as the sensitivity of some runs to cloud-droplet sedimentation.

2. Case Setup

[7] DYCOMS-II RF02 sampled a cylindrical column of 30 km radius in the marine boundary layer during a 5-h nighttime period, following it in an approximate Lagrangian trajectory as it was advected by the horizontal winds. Despite the significant horizontal variations in drizzle, the boundary layer liquid water potential temperature, θ_l, and the total specific humidity, q_t, were fairly horizontally and vertically uniform [see *vanZanten and Stevens*, 2005]. The boundary layer in RF02 was capped by a temperature inversion of about 8 K. The intercomparison simulations are initialized with idealized boundary layer profiles based on the RF02 mean conditions.

[8] The RF02 case specifications and requested outputs can be found at the GCSS BLCWG homepage at http://www.convection.info/blclouds/. The SCM case specifications are detailed below.

[9] To facilitate model setup and analysis and to minimize differences between models other than moist physics and turbulent transport, several aspects of the observations were slightly idealized from the RF02 observations and standardized across SCMs. These include the initial temperature and moisture profiles, the geostrophic wind profiles, the surface fluxes, and the radiative fluxes. Informal sensitivity studies have suggested to us that these idealizations do not have large impacts on the SCM results.

[10] The RF02 observations included segments of open cell convection and of more uniform closed cell convection with different statistical properties [*vanZanten and Stevens*, 2005].

[11] The initial profiles of θ_l and q_t, and horizontal winds u and v are specified as:

$$\theta_l = \left\{ \begin{array}{c} 288.3 \text{ K, if } z < z_i \\ 295 + (z - z_i)^{1/3} \text{ K, otherwise} \end{array} \right\} \tag{1}$$

$$q_t = \left\{ \begin{array}{c} 9.45 \text{ g kg}^{-1}, \text{if } z < z_i \\ 5 - 3\left(1 - e^{(z_i - z)/500}\right) \text{g kg}^{-1}, \text{otherwise} \end{array} \right\} \tag{2}$$

$$u = 3 + 4.3\,z/1000 \text{ m s}^{-1} \tag{3}$$

$$v = -9 + 5.6\,z/1000 \text{ m s}^{-1} \tag{4}$$

where z_i = 795 m is the inversion height and z is the height in meters. The geostrophic winds are maintained at the initial values of u and v throughout the simulation using the coriolis parameter at 31.5°N. Advective forcing due to subsidence is imposed on the basis of a vertical velocity of $w = -Dz$ with constant divergence $D = 3.75 \times 10^{-6}\text{s}^{-1}$ identical to the value used in the RF01 intercomparison [*Stevens et al.*, 2005]. While there is a high degree of observational uncertainty in D, this value is chosen value to maintain an approximate balance between radiative cooling and subsidence warming above the inversion. On the basis of observed mean RF02 values from *vanZanten and Stevens* [2005], a constant surface latent heat flux of 93 W m^{-2} and sensible heat flux of 16 W m^{-2} are maintained throughout the simulation. The upward surface zonal momentum flux is specified from the lowest model level u and v as

$$\overline{w'u'} = \frac{uu_*^2}{\sqrt{u^2 + v^2}} \tag{5}$$

where the friction velocity u_* is fixed at 0.25 m s^{-1}, and a similar expression holds for meridional momentum flux.

[12] As in the work by *Stevens et al.* [2005] and explored by *Larson et al.* [2007], the specified net (upward minus downward) radiative flux is based on liquid water path and inversion height

$$F(z) = F_0 e^{-Q(z,\infty)} + F_1 e^{-Q(0,z)} + \alpha \rho_i C_p D \cdot \left[0.25(z - z_i)^{4/3} + z_i (z - z_i)^{1/3}\right] H(z - z_i), \tag{6}$$

where

$$Q(z_1, z_2) = \kappa \int_{z_1}^{z_2} \rho q_l dz, \tag{7}$$

$\kappa = 85\,\text{m}^2\,\text{kg}^{-1}$, $F_0 = 70\,\text{W m}^{-2}$, $F_1 = 22\,\text{W m}^{-2}$, $\alpha = 1\,\text{K m}^{1/3}$, ρ is the air density, ρ_i = 1.12 g m^{-3} is the initial air density

Table 1. Summary of Participating Models

Model	*Investigator*	*Turbulence*	*Autoconversion Type*	*Evaporation Type*	*Cloud Fraction*	*Standard-Resolution Levels < 1 km*	*High-Resolution Levels < 1 km*
CAM 3	C.-L. Lappen, S. Park	nonlocal, K profile, surface-based	*Chen and Cotton* [1987]	*Sundqvist et al.* [1989]	RH, convective mass flux, or lower-tropospheric stability	5	100
CAM 3-UW	C.-L. Lappen, S. Park	K profile, explicit w_e	*Chen and Cotton* [1987]	*Sundqvist et al.* [1989]	same as CAM w/o lower-tropospheric stability	5	100
KNMI-RACMO/ ECMWF-CY23R4	S. de Roode	K profile, explicit w_e	*Sundqvist et al.* [1989]	*Tiedtke* [1993]	*Tiedtke* [1993]	10	96
GFDL AM2.12b	M. Zhao	nonlocal, K profile, explicit w_e	*Tripoli and Cotton* [1980]	*Rotstayn* [1997]	*Tiedtke* [1993]	7	113
JMA	H. Kitagawa	nonlocal, K profile	*Sundqvist et al.* [1989]	*Tiedtke* [1993]	RH-pdf	5	100
MPI ECHAM4/5	A. Chlond	moist TKE, explicit w_e	*Sundqvist et al.* [1989]	*Sundqvist et al.* [1989]	pdf	10	–
UKMO	A. Lock	nonlocal, K profile, explicit w_e	*Tripoli and Cotton* [1980]	*Wilson and Ballard* [1999]	RH-pdf [*Smith*, 1990]	11	–
UWM and UWM-sed	B. Griffin, V. Larson	prognostic $\overline{w'^2}$, $\overline{w'^3}$, $\overline{w'\theta_l}$, $\overline{w'q_t}$	*Khairoutdinov and Kogan* [2000]	*Khairoutdinov and Kogan* [2000]	pdf	10	100
MLM and MLM-sed	J. Uchida, C. Bretherton	explicit w_e	Caldwell and Bretherton (submitted manuscript, 2007)	Caldwell and Bretherton (submitted manuscript, 2007)	–	–	–
DHARMA LES	A. Ackerman	resolved to grid scale with dynamic Smagorinsky subgrid scale [*Kirkpatrick et al.*, 2006]	bin microphysics including cloud droplet sedimentation	bin-resolved	fraction of columns with LWP > 20 g m^{-2}	86	–

at the inversion, q_l is the liquid water content, C_p is the specific heat of air at constant pressure, H is the Heaviside step function, and z_i, the inversion height, is defined as the height where $q_t = 8$ g kg^{-1}.

[13] The cloud droplet concentration, N, is specified as 55 cm^{-3} as discussed in A07. As the radiation is idealized, this specification only affects the simulations through its impact on drizzle processes. Some of the SCMs use precipitation parameterizations without an explicit dependence on droplet concentration and could not make use of this specification.

[14] All simulations were integrated for 6 h. To better understand the impact of vertical model resolution, simulations were performed for most SCMs at two vertical and time resolutions. The "standard" resolution is intended to represent the typical operational vertical resolution in the host large-scale model, which varies between models. The "high-resolution" runs have a specified vertical resolution of 10 m and a typical time step of order 10 s.

[15] To isolate the impact of drizzle on simulated MBL evolution, additional sensitivity experiments were run by most SCMs in which the drizzle parameterization was turned off. For models that use cumulus parameterizations, sensitivity experiments were also performed with these turned off. However, for most models, either the cumulus parameterization had little or no impact on the results or it could not be easily inactivated, so these results are not presented here.

[16] For two models additional experiments were performed using cloud-droplet- sedimentation flux parameterized as

$$F_{sed} = c\left(\frac{3}{4\pi\rho_l N}\right)^{2/3}(\rho q_l)^{5/3}\exp\left(5\ln^2\sigma_g\right) \tag{8}$$

where ρ_l is the density of liquid water, and $c = 1.19 \times 10^8$ m^{-1} s^{-1}. This is based on a lognormal size distribution of cloud droplets with geometric standard deviation $\sigma_g = 1.5$ falling in a Stokes regime.

[17] After a preliminary intercomparison, the experiment was revised slightly and participants were able to make corrections or adjust their models, before submitting the final intercomparison results presented here.

3. Single-Column Model Descriptions

[18] The seven SCMs participating in this study represent many of the world's leading climate models. Several of the same models participated in the intercomparison of Z05. In this study, we also include mixed layer model (MLM) results. The model physics of the SCMs, the MLM, and the LES model used in this study are summarized in Table 1. Participating models included a single-column version of the National Center for Atmospheric Research Community Atmosphere Model (CAM) GCM, version 3.0 [*Collins et al.*, 2006], and a variant, CAM-UW, which has identical microphysics, a slightly simpler cloud fraction scheme, and a different moist turbulent mixing and shallow cumulus convection scheme [*Bretherton et al.*, 2004a]. The third participating SCM was the Royal Netherlands Meteorological Institute (KNMI) Regional Atmospheric Climate Model

(RACMO) single-column model [*Lenderink et al.*, 2003] with physical parameterizations identical to the CY23R4 version of the European Centre for Medium-Range Weather Forecasts (ECMWF) model. The Geophysical Fluid Dynamics Laboratory (GFDL) submitted results from a single-column version of the GFDL AM2.12b atmospheric GCM [*Anderson et al.*, 2004]. The SCM derived from the Japan Meteorological Agency (JMA) model is described by *Kitagawa et al.* [2007]. The Max Planck Institute (MPI) model used here [*Chlond et al.*, 2004] is a modified experimental version of the ECHAM4/5 SCM [*Roeckner et al.*, 1996, 2003]. The UK Met Office SCM (UKMO) is based on the current UKMO forecast model and is very close to the model used in HadGEM1 [*Martin et al.*, 2006]. The model of University of Wisconsin-Milwaukee (UWM) is a third-order turbulence closure model based on *Golaz et al.* [2002] and *Larson and Golaz* [2005]. This model was also run with a cloud-droplet sedimentation scheme operating (UWM-sed).

[19] The University of Washington MLM [*Bretherton and Wyant*, 1997] uses the *Turton and Nicholls* [1987] entrainment closure at cloud top. A new observationally derived drizzle parameterization (P. Caldwell and C. S. Bretherton, Response of a subtropical stratocumulus-capped mixed layer to climate and aerosol changes. Part I: Model design and numerical results, submitted to *Journal of Climate,* 2007, hereinafter referred to as Caldwell and Bretherton, submitted manuscript, 2007) has been added. The MLM-sed simulations include sedimentation corrections to the buoyancy flux profile and the entrainment closure [*Bretherton et al.*, 2006].

[20] As a baseline for comparison, we use results from the DHARMA LES [*Stevens et al.*, 2002] with a bin microphysics scheme [*Ackerman et al.*, 1995] in which aerosol composition and size distributions are specified so as to approximately match the cloud-droplet concentration that was specified for this case [A07]. The bin microphysics scheme incorporates both drizzle and cloud-droplet sedimentation process. As discussed by A07, these simulations agree comparatively well with the RF02 observations of both turbulent and microphysical fields. The fluid dynamics of DHARMA are described by *Stevens et al.* [2002]. The model LES was run in a horizontally periodic domain of 6.4 km $\times$ 6.4 km with 50 m $\times$ 50 m horizontal resolution. The vertical resolution varied from 5 m near the surface and near the inversion to 20 m in the middle of the boundary layer.

[21] Among the SCMs there is a variety of methods for representing turbulent processes. The CAM uses a nonlocal K profile-based scheme [*Holtslag and Boville*, 1993] driven only by surface fluxes. Unlike the other models, CAM does not take moist processes (such as condensation in stratocumulus) directly into account its turbulent flux parameterization. Several models (CAM-UW, KNMI, JMA) use K profile-based down-gradient diffusion of moist-conserved variables in the interior of a turbulent layer. The MPI model uses a TKE-type closure. The UWM and UWM-sed models use a turbulence scheme that prognoses $\overline{w'^2}$, $\overline{w'^3}$, $\overline{w'\theta_l'}$, and $\overline{w'q_l'}$ and closes these equations using a multivariate probability density function. Both the UKMO and GFDL models use the *Lock et al.* [2000] nonlocal turbulent mixing scheme, which specifies various types of K profiles based on surface fluxes and cloud top radiative forcing for different boundary layer cloud regimes. All models except JMA, CAM, UWM and UWM-sed use an explicit inversion-top entrainment rate, w_e, that has some dependence on stratocumulus-top longwave cooling. The SCMs use a variety of vertical advection schemes.

[22] In the SCMs, drizzle is produced by autoconversion and collection. The autoconversion production is largest near stratocumulus cloud top where liquid water content is the largest and plays a primary role in determining cloud base precipitation. Most models produce additional drizzle by the collection of cloud droplets by drizzle droplets but this drizzle source is dependent on autoconversion rates. Here we compare the scaling of autoconversion in the models, assuming the cloud fraction is unity. The JMA, MPI, and KNMI models use the microphysics scheme of *Sundqvist* [1978] and *Sundqvist et al.* [1989] in which the autoconversion rate scales as $A : q_l\,(1-\exp\{-(q_l\,/\,q_{lcrit})^2\})$ where q_{lcrit} is a constant typically of similar magnitude to stratocumulus cloud top q_l. For small q_l relative to q_{lcrit}, this relationship scales as $A : q_l^3$. Models using this scheme could not make use of the cloud droplet concentration specified for this case. The GFDL and UKMO models all have similar autoconversion scaling as *Tripoli and Cotton* [1980] with $A : q_l^{7/3}\ N^{-1/3}H\ (q_l - q_{lcrit})$, where H is the Heaviside step function. CAM and CAM-UW similarly have $A : q_l^{7/3}\ N^{-1/3}H\ (r - r_{crit})$ based on *Chen and Cotton* [1987] where r is the mean cloud droplet radius and r_{crit} is a constant. CAM and CAM-UW have an additional factor as low as 0.1 which multiplies autoconversion when precipitation rates are less than 0.5 mm d^{-1}. UWM and UWM-sed use microphysics from the empirically based *Khairoutdinov and Kogan* [2000] which has $A : q_l^{2.47}\ N^{-1.79}$. The mixed layer model does not specify autoconversion rate, but instead directly specifies cloud base precipitation rate that scales with $(LWP/N)^{1.75}$. Even models with similar parametric forms can behave quite differently on the basis of choice of constants. Only the UWM-sed and MLM-sed models include a parameterization of cloud-droplet sedimentation.

[23] Evaporation of drizzle below cloud base is determined by many aspects of the microphysics, including assumed rainfall drop-size distribution and droplet fall speed parameterizations, but many of the models' evaporation rates scale similarly. For purposes of comparison we assume zero cloud fraction below stratocumulus cloud base and 100% area coverage of drizzle. In CAM, CAM-UW and MPI, the evaporation rate follows *Sundqvist et al.* [1989] and scales as $E : -SP^{0.5}$, where P is the precipitation flux. $S = (q_v/q_{vsat} - 1)$ is the water vapor supersaturation (q_{vsat} is the saturation specific humidity) so $-S$ is positive and represents the degree of subsaturation. JMA and KNMI use the *Tiedtke* [1993] evaporation scheme with $E : -SP^{0.577}$. The GFDL model follows *Rotstayn* [1997] with $E : -SP^{0.61}$. In the UWM and UWM-sed models, $E : -Sq_r^{1/3}\ N_r^{2/3}$, where N_r is the drizzle droplet concentration [*Kharoutdinov and Kogan*, 2000]. Using the approximate scaling $P : q_r^{4/3}$ and $N_r : q_r$ gives $E : -SP^{0.75}$. The UKMO model uses the precipitation scheme of *Wilson and Ballard* [1999], and evaporation scales as $E : -S(q_r^{0.177} + 60q_r^{0.518})$ where q_r is the rainwater mixing ratio (D. Wilson, personal communication, 2007). The latter term dominates for large drizzle rates. The MLM does not diagnose evaporation, but instead

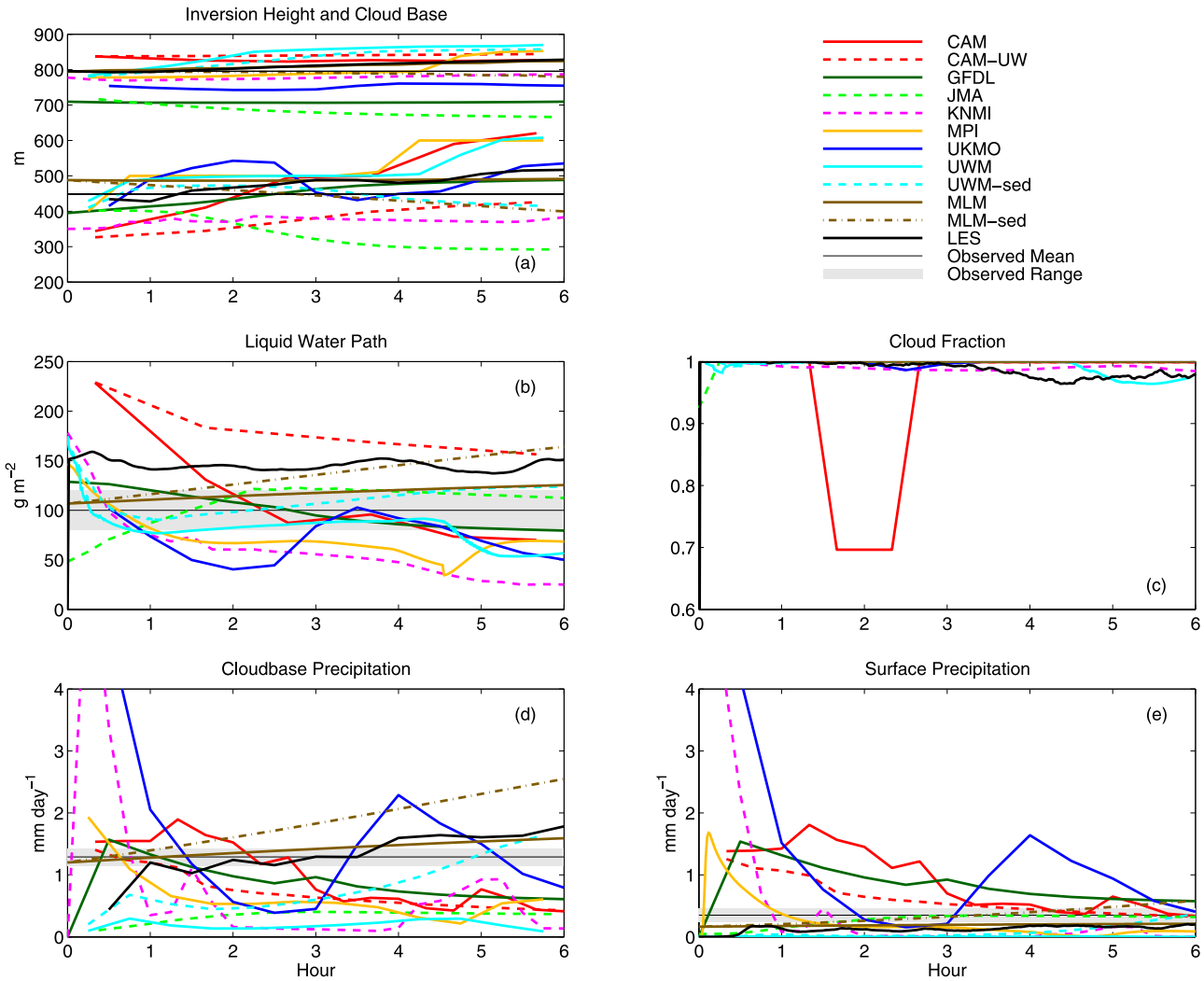

Figure 1. Evolution of (a) inversion height and cloud base, (b) liquid water path, (c) cloud fraction, (d) cloud base precipitation, and (e) surface precipitation for the standard-resolution case. Also plotted is the evolution of DHARMA LES (thick black lines), observed mean values (thin black line) and uncertainty range of observations (gray shading). Observed values of inversion height and cloud base (LCL) are from *vanZanten and Stevens* [2005], and values of precipitation are from *vanZanten et al.* [2005].

specifies precipitation rate based on the distance below cloud base: $P : P_{zb} \exp(-k(z_b - z)^{1.5})$, where z_b is the cloud base height, P_{zb} is the cloud base precipitation rate, and k is a constant (Caldwell and Bretherton, submitted manuscript, 2007).

[24] For most of the SCMs, cloud fraction is determined using a pdf approach based on layer mean relative humidity (JMA, MPI, UWM, UWM-sed, and UKMO). The CAM takes cloud fraction as the maximum of three estimates based on local relative humidity, lower-tropospheric stability [*Klein and Hartmann*, 1993], and parameterized shallow and deep convection. CAM-UW is similar, but does not include the lower-tropospheric stability estimate. The KNMI and GFDL models use the cloud fraction as prognosed by the *Tiedtke* [1993] cloud fraction scheme. In the LES, the cloud fraction is diagnosed as the fraction of columns with liquid water path >20 g m^{-2}. Note that for the SCMs, the cloud fraction is not used by the simplified radiation scheme.

[25] The SCM vertical resolution in the standard runs varies somewhat, with the JMA, CAM, and CAM-UW models having 5 grid levels below 1 km, GFDL having 7 such levels, and the rest of the models having 10 or 11 such grid levels. The SCM high-resolution runs have 100 or more levels below 1 km, giving 10-m or better typical vertical grid spacing, similar to the DHARMA LES.

[26] Similar versions of the CAM, CAM-UW, MPI, UKMO, and the UWM SCMs were used in the RF01 comparison of Z05. The CAM boundary layer and cloud physics are largely unchanged from that study. CAM-UW has been substantially developed and tuned compared to the earlier study, though much of the physics remains the same. The UWM model uses a different turbulent length scale but is otherwise similar to the NRL model presented there. The MPI and UKMO models are basically unchanged. The KNMI model is related to the ECMWF model used in Z05. but that model used a significantly different boundary layer scheme (ECMWF C29R1). The KNMI model also

Table 2. Comparison of Entrainment Rate, w_e, and Liquid Water Path, *LWP*, for the Final Two Simulation Hours for Both Standard and High-Resolution Experiments[a]

Experiment	CAM	CAM-UW	GFDL	JMA	KNMI	MPI	UKMO	UWM	UWM-sed	LES	MLM	MLM-sed	Observed
Standard resolution													
w_e	0.41	0.36	0.30	0.15	0.37	0.68[b]	0.20	0.43	0.41	0.45	0.45	0.17	0.60–0.76
LWP	76	162	81	116	30	58	65	69	121	144	123	155	100 ± 20
High resolution													
w_e	0.37	0.45	0.30	0.79	0.75	0.62	–	0.77	0.63				
LWP	108	85	147	61	73	66	–	67	111				

[a]Unit of w_e is cm s^{-1}, and unit of *LWP* is g m^{-2}.
[b]Estimated from full 6 h because of jump in inversion height in final 2 h.

differs from the prognostic moist-TKE model presented as the KNMI model in Z05.

4. Experiment Results

4.1. Standard-Resolution Case

[27] Figure 1 shows the 6-h evolution of inversion height, cloud base, liquid water path (LWP), cloud fraction, and precipitation at cloud base and at the surface for the standard-resolution SCMs. The inversion height is found by interpolating between levels to the height where q_t drops to 8 g kg^{-1}. The cloud base is determined by interpolating to find the lowest level where cloud fraction reaches 0.5. The initial intermodel variability in inversion height, cloud base height, and LWP is largely due to the projection of the specified initial sounding onto the coarse standard-resolution grid. All the models maintain a fairly well mixed stratocumulus-topped boundary layer. Their simulated cloud fractions (Figure 1c) remain near unity except for a short period around hour 2 in CAM. We will avoid comparison within the first 2 h of simulation, when many models display large transients.

[28] After 2 h, the inversion height, which is nearly coincident with cloud top in each model, rises gradually for most models. In the JMA and MLM-sed runs, the inversion height lowers. At standard resolution, diagnosing the evolution of inversion height is somewhat imprecise and method-dependent, but we choose the q_t inversion method to provide some consistency across models. The change in inversion height together with the specified subsidence profile is used to calculate the entrainment rate, w_e averaged over the final two simulation hours (Table 2, first row). The tabulated w_e values at standard resolution have an estimated uncertainty of ±0.1 cm s^{-1}. The SCMs' w_e ranges from 0.15 to 0.68 cm s^{-1}, with all models except MPI lower than the observed range of 0.60–0.76 cm s^{-1} [*Faloona et al.*, 2005].

[29] The cloud base height has a larger range of responses than inversion height, spanning 300 m by the end of hour 6, resulting in a broad range of simulated LWP (Figure 1b). An estimate of the average mean observed LWP of 100 g m^{-2} (based on M. van Zanten (personal communication, 2005) and *Stevens et al.* [2003]) is plotted. The mean LWP of the final 2 h (also see Table 2, second row) varies by more than a factor of 5 between models, ranging from 30 g m^{-2} to 162 g m^{-2}, with numerous models both below and above the RF02 observed mean. SCM Runs with no precipitation display an even larger spread of LWP values, so we attribute this LWP spread mainly to differences in turbulence parameterization and not microphysical parameterization between models. Turbulence parameterization affects both the entrainment rate and the moisture stratification in the boundary layer [*Stevens et al.*, 2005; *De Roode*, 2007] both of which can strongly affect LWP. For comparable models' precipitating runs in both RF01 and RF02 studies, the RF02 LWP ranges from 80 to 250% of that in RF01. This mostly larger LWP despite much stronger in precipitation in RF02 is probably due the moister conditions above the inversion in RF02.

[30] After hour 2, the cloud base precipitation rate (Figure 1d) remains weaker than the mean observed value [*vanZanten et al.*, 2005] for most SCMs. The mean surface precipitation rate (Figure 1e) after hour 2 is less than 1 mm d^{-1} for most SCMs, though for a few models it is stronger than the mean observed surface precipitation rate of 0.35 mm d^{-1} [*vanZanten et al.*, 2005]. (The GFDL precipitation flux peaks well below cloud base indicating substantial precipitation production at levels with low cloud fraction. This study will use the GFDL precipitation flux at the level where it reaches a maximum, typically about 150 m, in place of its cloud base precipitation flux.) The relation between precipitation and LWP will be explored in the next section.

[31] Figures 2a and 2b show initial profiles of q_t and θ_l (thin black lines) and SCM, MLM and LES final profiles. For all models, q_t and θ_l are nearly constant with height, indicating a well-mixed MBL at simulation end. The boundary layer q_t does not vary too far from the initial 9.45 g kg^{-1} for all the SCMs, except for the JMA and MLM-sed models. The JMA model moistens by 0.8 g kg^{-1} in the lower boundary layer, and the MLM-sed boundary layer q_t moistens by 0.5 g kg^{-1}. Such moistening is due to the relative lack of entrainment drying in these models. There is a θ_l increase ranging from 0 to 1.2 K across the models, strongly positively correlated with the models' entrainment rate. There is little θ_l stratification except in the KNMI model, in which θ_l warms in the cloud layer by up to 1.8 K. The coarse vertical resolution in the SCMs smears out their inversion layers compared to the LES and observations.

[32] In Figure 2c, the cloud liquid water profiles are compared. Also plotted is the peak of the mean observed liquid water profile in RF02 [*vanZanten and Stevens*, 2005]. The models' peak liquid water is evenly scattered about the observed value. The low q_l in the KNMI run is probably connected to the elevated θ_l in the cloud layer. The MLM and MLM-sed runs have the largest peak q_l values because they assume adiabatic liquid water profiles up to the inversion, and the MLM-sed run entrains relatively weakly. All of the q_l profiles except for KNMI are optically thick with respect to the longwave radiation scheme.

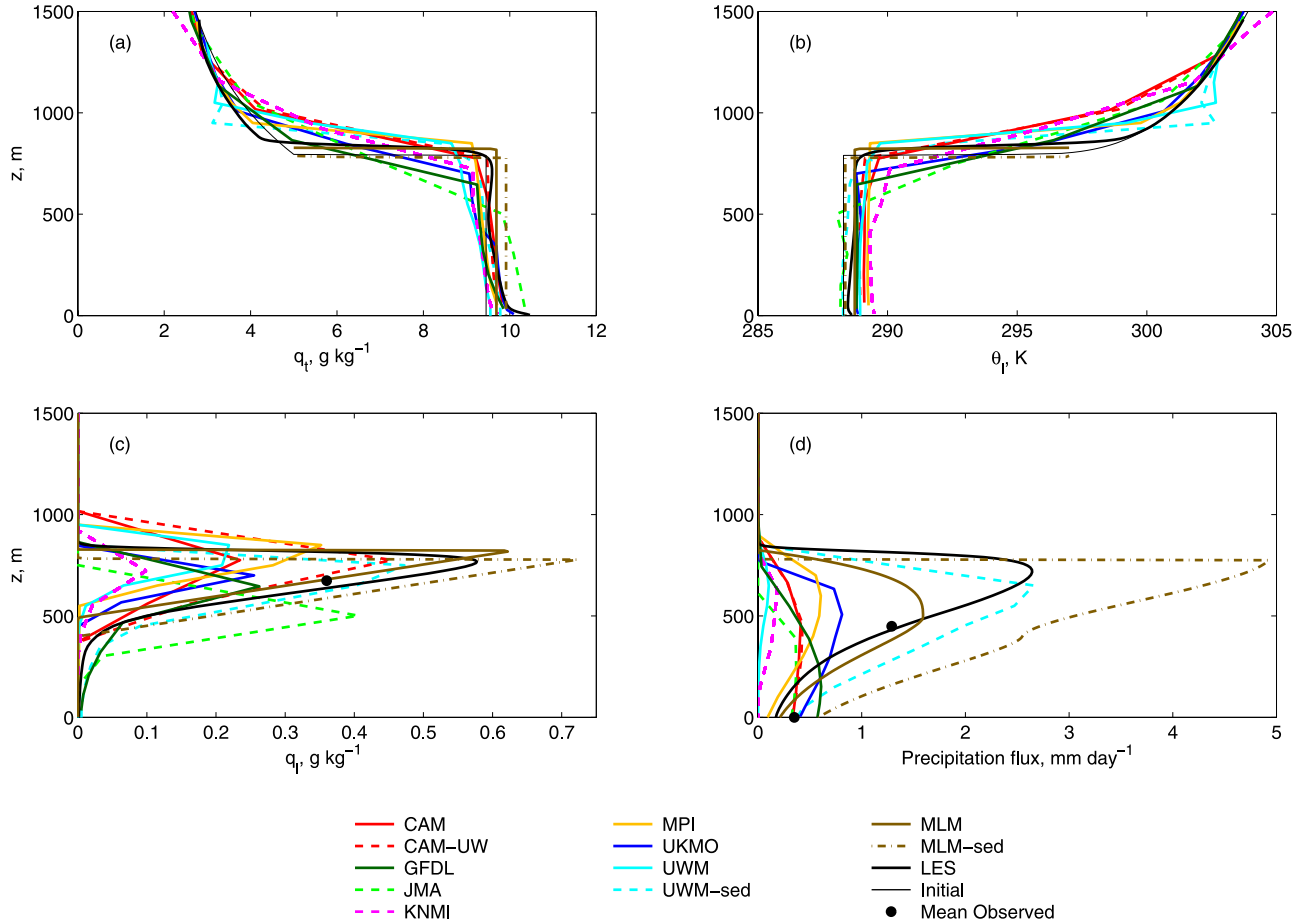

Figure 2. SCM and LES profiles at hour 6 of (a) total specific humidity, q_t; (b) liquid water potential temperature, θ_l; (c) cloud liquid water, q_l; and (d) precipitation flux. The initial profiles of qt and θ_l are plotted as thin black lines. The peak in the mean RF02 q_l profile [*vanZanten and Stevens*, 2005] and mean observed precipitation flux values at cloud base and at the surface are plotted as black dots [*vanZanten et al.*, 2005].

[33] The precipitation flux is plotted in Figure 2e together with mean RF02 estimates at the surface and at cloud base. Most models substantially underestimate cloud base precipitation by a factor of two or more. The few models with cloud base precipitation larger than observed also show strong evaporation below cloud base, greatly reducing the spread of modeled surface precipitation rate.

4.2. High-Resolution Case

[34] A high-resolution simulation was submitted for all SCMs except UKMO. For most models the results are broadly similar to the standard-resolution case, though there are some substantial differences. As was the case in Z05, the entrainment rate (see Table 2, third row) is larger for most models at higher resolution. This places several models closer to the observed entrainment rate. Each of the JMA, KNMI, UWM, and UWM-sed models' w_e during the final 2 h is more than 50% larger in the high-resolution case than in its respective standard-resolution case. Except for KNMI, these models do not use explicit entrainment parameterizations, which may explain their high sensitivity to vertical resolution. The spread in entrainment rate across models is quite large.

[35] At high resolution, the inversion is much better resolved, so the cloud water profiles tend to be much closer to adiabatic as observed. However, the spread in LWP (Table 2, fourth row) across SCMs is quite large (61–147 g m^{-2}), and some models show large LWP differences between their standard and high-resolution runs. At high resolution CAM-UW and JMA have much lower LWP, while the GFDL and KNMI and CAM have much higher LWP. Most of the models with large (>40%) changes in LWP were models with less vertical resolution in the standard runs.

[36] There is little impact of vertical resolution on simulated cloud fraction (not shown). Cloud fraction remains near 100% for all models at high resolution except for the JMA model where it lowers to about 88% at the end of 6 h. Discussion of the effects of precipitation on the high-resolution runs is included below.

5. Comparison of Precipitation Between the Models

[37] The precipitation differences between the SCM simulations are connected to both differing liquid water profiles and differing parameterizations of precipitation production

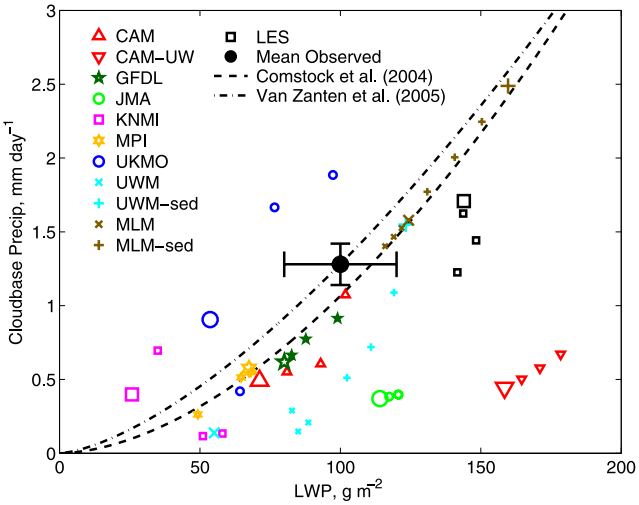

Figure 3. Mean cloud base precipitation and liquid water path for the SCMs at standard resolution, the MLM, and the LES. For each model the large symbol represents the hour 6 mean, and the smaller symbols represent the means for hours 3, 4, and 5. The observed mean RF02 value is plotted with uncertainty bars. Empirical relations between LWP and cloud base precipitation are plotted as dashed and dashed-dotted lines.

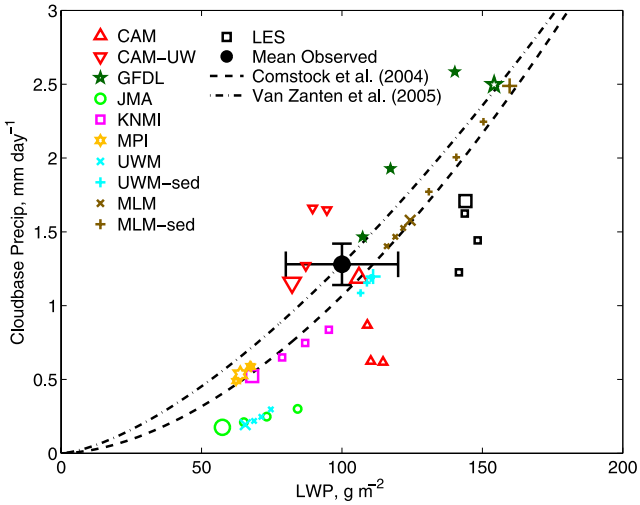

Figure 4. Same as Figure 3 except for high-resolution case. UKMO did not submit a high-resolution simulation. LES and MLM runs are identical to those shown on Figure 3.

and subcloud evaporation. Our focus in this section is precipitation parameterization differences.

[38] To control for the large intermodel LWP variations, we start by comparing the relationship in different models between liquid water path and cloud base precipitation. Figure 3 shows the relation between average cloud base precipitation and LWP for the standard-resolution model runs. For each model, each of the hour 3, 4, and 5 means is plotted with a small symbol, and the hour 6 mean is plotted with a large symbol. The observed mean RF02 value is also plotted as a large filled black circle with uncertainty bars. Empirical fits of cloud base precipitation to LWP given the case-specified droplet concentration are plotted on the basis of field observations from EPIC (long dashed line, *Comstock et al.* [2004]) and DYCOMS-II (dash-dotted line). The DYCOMS-II fit was estimated from *vanZanten et al.* [2005] utilizing the approximately linear relation between cloud base precipitation and H^3N^{-1} where H is the mean cloud thickness, and assuming the cloud LWP is 71% of adiabatic value, as was approximately the case in RF02. Since the microphysical schemes of most SCMs were not developed for or calibrated to stratocumulus drizzle, the general consistency between SCMs and observations is encouraging. Most of the SCMs do show a clear correlation between LWP and precipitation as expected. GFDL and MPI show excellent agreement with the empirical fits, though other models scatter considerably around these fits. Note that the MLM's drizzle scheme is based on the *Comstock et al.* [2004] empirical fit.

[39] Figure 4 shows cloud base precipitation compared to LWP for the high-resolution cases. The scatter of the models about the empirical fit is significantly reduced, with closer fits for the CAM-UW, UWM-sed, especially the KNMI model. Comparison with Figure 3 also shows the strong resolution dependence of precipitation for some models. The GFDL model has strong increases in LWP and cloud base precipitation compared with the standard-resolution case. Interestingly the CAM-UW model produces more precipitation at cloud base than the low-resolution case despite much lower LWP. This behavior is not well understood. Further experiments have shown that precipitation in CAM-UW is highly sensitive to changes in implementation details of the CAM microphysics scheme and its integration with other model components.

[40] The evaporation of drizzle before it reaches the surface is also important for the MBL water budget and turbulence dynamics. Using differences in precipitation flux profiles from cloud base to the surface we infer the evaporation rate below cloud base. Figure 5 shows the partitioning of the subcloud precipitation rate averaged over

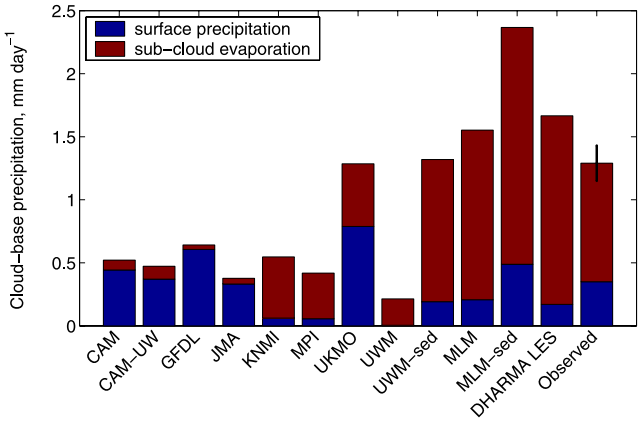

Figure 5. Mean cloud base precipitation rate for the last two simulation hours of the standard case as compared with mean RF02 observations. This rate is partitioned into mean surface precipitation rate (blue) and the subcloud evaporation rate (red). Uncertainty in observed cloud base precipitation is plotted as a black line.

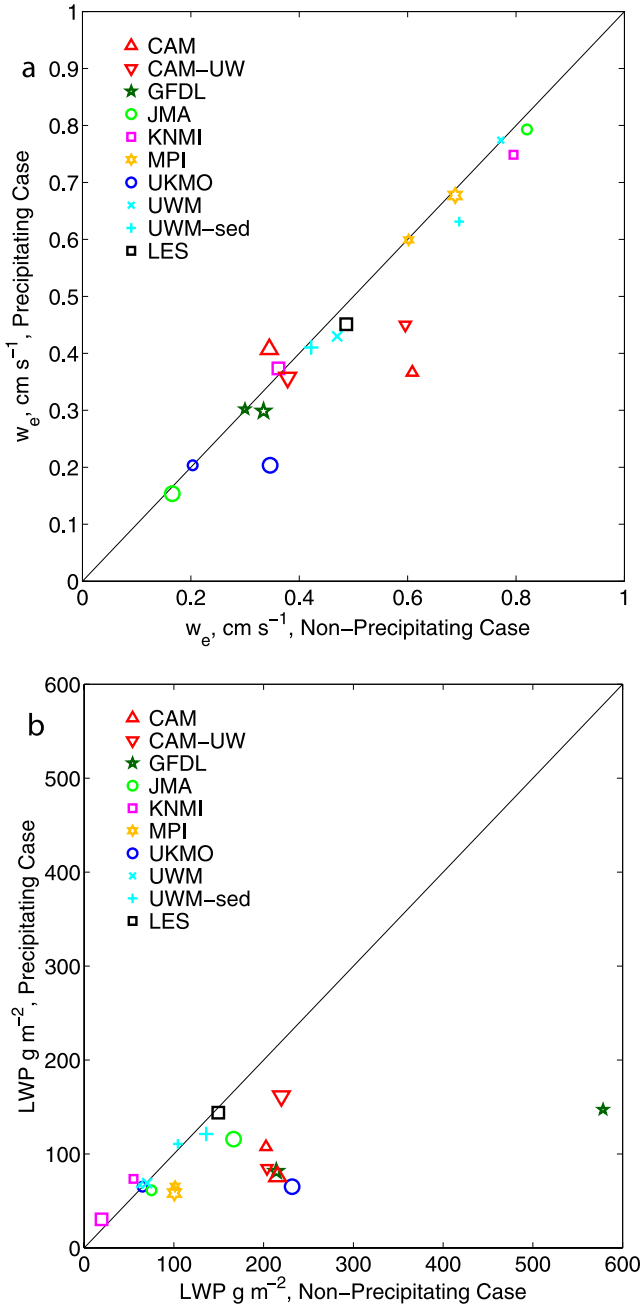

Figure 6. (a) Mean entrainment rate over the final two simulation hours, with symbols as in Figure 3. For the SCMs the larger symbol indicates standard-resolution run and the smaller symbol, when present, indicates the high-resolution run. The thin black line represents no difference between precipitating and nonprecipitating cases. (b) Same as Figure 6a except with liquid water path.

the final two simulation hours into precipitation that evaporates below cloud base (red) and precipitation that reaches the surface (blue). The large observed fraction of evaporating precipitation (73%, based on 5-h means) is consistent with 30 min flight leg mean estimates that range from 63% to 98% in RF02 [*vanZanten et al.*, 2005]. In the DHARMA LES, MLM, MLM-sed, UWM, and UWM-sed runs, most of the precipitation evaporates, as observed. In contrast, CAM, CAM-UW, GFDL, JMA and to a lesser extent UKMO allow much of the cloud base precipitation to reach the surface, resulting in net boundary layer heating and drying. The different SCM evaporation scaling relations shown earlier are quite similar for many models, though choice of constants (tuning) could alone account for large differences between models. For JMA, a low cloud base and a relatively moist boundary layer contributes to the underestimate. The GFDL inferred evaporation is also likely underestimated because of the use of precipitation at its maximum level below cloud base instead of at cloud base. An additional source of differences is the handling of fractional cloudiness in evaporation schemes and the extent to which models maintain nonzero cloud fraction below the main stratocumulus deck.

[41] To assess the impact of precipitation on the simulations, we compare the standard runs with nonprecipitating runs performed by all of the SCMs and by DHARMA. Note that both the DHARMA precipitating and nonprecipitating runs include a cloud-droplet sedimentation process. The former uses bin-resolved sedimentation and the latter uses equation (8). Figures 6a and 6b compare the average entrainment rate and the LWP over the final two simulation hours for the precipitating runs versus their nonprecipitating counterparts. For each model the larger symbol represents the standard-resolution case, and the smaller symbol represents the high-resolution case, if available (the thin black line indicates no difference between the precipitating and nonprecipitating cases). For most models and runs, the entrainment rate is affected only slightly or not at all by precipitation. Where there is an effect, the precipitation appears to decrease entrainment rate compared to the nonprecipitating case. Previous LES, mixed layer model, and theoretical work have shown that drizzle stabilizes the upper boundary layer because of net condensational heating. This in turn causes weaker turbulent eddies and less entrainment at cloud top. The difference in entrainment is particularly pronounced for the CAM and CAM-UW high-resolution runs and the UKMO run standard-resolution run. The cloud base precipitation in these models are all comparable to or above the observational estimate. Conversely, many of the other models whose w_e is not sensitive to drizzle have cloud base precipitation rates far less than observed.

[42] The LWP response to precipitation is much more diverse (Figure 6b). A majority of the SCM run pairs show a substantial reduction in LWP (>25%) due to precipitation. The sensitivity of LWP to inclusion of precipitation is much stronger than that seen in the weakly precipitating RF01 case [Z05]. The LES LWP is also reduced by drizzle but the effect is also weaker than for most of the SCMs.

6. Effect of Droplet Sedimentation

[43] The LES results of *Ackerman et al.* [2004] and *Bretherton et al.* [2006] suggest that cloud-droplet sedimentation at the top of the stratocumulus-topped MBL causes a significant reduction in entrainment. The corresponding reduction of entrainment drying can cause LWP to increase.

[44] In our intercomparison, there are several pairs of runs with parameterized sedimentation turned on and off. In addition to MLM and MLM-sed, and UWM and UWM-sed, we also consider the control LES run together with a

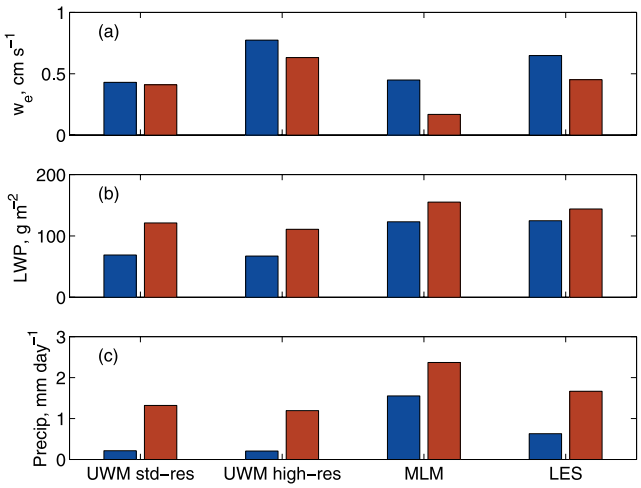

Figure 7. A comparison of runs without (blue) and with (red) droplet sedimentation for four model configurations: UWM at standard resolution, UWM at high resolution, the mixed layer model (MLM), and the DHARMA LES. Plotted are final 2 h averages of (a) entrainment rate, (b) liquid water path, and (c) cloud base precipitation.

LES run with cloud-droplet sedimentation disabled. The final 2-h averages of entrainment rate, liquid water path, and cloud base precipitation for these runs are shown in Figure 7. In all four cases, inclusion of sedimentation has the expected effects of reducing the entrainment rate, increasing the liquid water path, and increasing the precipitation rate.

[45] The value σ_g = 1.5 used in the sedimentation parameterization (equation (8)) may represent an unrealistically broad cloud droplet distribution for this case. RF02 observations give an estimated σ_g = 1.2 (M. van Zanten, personal communication, 2005), which would reduce the parameterized sedimentation fluxes by about a factor of 2. Thus the substantial effects of sedimentation shown here are possibly exaggerated.

7. Discussion and Conclusions

[46] As with earlier SCM intercomparisons of thinner nonprecipitating stratocumulus, there is a large spread in LWP predicted by the models and the LWP is generally quite sensitive to the vertical resolution used. The range of simulated entrainment rates is larger than that of *Zhu et al.* [2005] and the observational agreement is not as good.

[47] The high liquid water content and low droplet concentration of the RF02 case leads to significant cloud base drizzle in all SCMs. Drizzle reduces entrainment in most models and produces a net reduction in LWP which can be very substantial. Parameterized sedimentation also causes a substantial decrease in entrainment but increases LWP. Many SCMs underestimate the fraction of drizzle evaporated beneath cloud base.

[48] Changing the vertical resolution has significant effects on many models. For many models higher resolution improves the agreement of entrainment rate with observation. Furthermore, the overall spread of model results is slightly reduced and the profile of cloud liquid water is somewhat more realistic in most SCMs.

[49] There are clearly many challenges associated with representing heavily drizzling stratocumulus within a single-column framework. Even if the drizzle and sedimentation fluxes are parameterized well, inaccuracies in resolution of cloud liquid water will result in substantially inaccurate drizzle flux. Subcloud evaporation must also be parameterized well to create a reasonably faithful simulation of the boundary layer. Most importantly, heavily drizzling stratocumulus layers can be highly horizontally inhomogeneous on large scales, an effect most SCMs do not attempt to account for. Heavy drizzle in stratocumulus is associated with convection organized into cellular structures such as POCs which have reduced cloud fraction. This association is found both in observations [*Comstock et al.*, 2005; *vanZanten et al.*, 2005], and LES modeling [*Savic-Jovcic and Stevens*, 2007]. In this study the SCMs' drizzle does not appear to have any substantial effect on cloud fraction.

[50] In the context of climate models, the sensitivities of the parameterized cloud microphysics to changing aerosol concentrations or warming temperatures are particularly important. Expected qualitative feedbacks of drizzle on entrainment and LWP are generally present in most SCMs, but testing and improving their quantitative accuracy and better accounting for horizontal heterogeneity remain major research problems.

[51] **Acknowledgments.** Thanks to Margreet van Zanten for assistance in interpreting the DYCOMS-II observations and to Damian Wilson for providing information about the UKMO model. Thanks also to the reviews of Bjorn Stevens and an anonymous reviewer which helped significantly improve this manuscript. M. Wyant and C. Bretherton were supported by National Science Foundation grants 0336703 and ATM-0433712. S. Park was supported by DOE grant DE-FG02-05ER63959 and NASA grant NNG05GA19G. B. Griffin and V. Larson are grateful for financial support from the National Science Foundation grant ATM-0442605. M. Zhao was supported under award NA17RJ2612 from the National Oceanic and Atmospheric Administration, U.S. Department of Commerce. The KNMI simulations were carried out in the framework the Dutch National Research Programme Climate changes Spatial Planning http://www.klimaatvoorruimte.nl). S. de Roode would like to acknowledge Martin Koehler for providing the single-column model of the C23R4 version of the ECMWF model. A. Ackerman was supported by NASA's Radiation Sciences Program.

References

Ackerman, A. S., O. B. Toon, and P. V. Hobbs (1995), A model for particle microphysics, turbulent mixing, and radiative transfer in the stratocumulus-topped marine boundary layer and comparisons with measurements, *J. Atmos. Sci.*, *52*, 1204–1236.

Ackerman, A. S., M. P. Kirkpatrick, D. E. Stevens, and O. B. Toon (2004), The impact of humidity above stratiform clouds on indirect aerosol climate forcing, *Nature*, *432*, 1014–1017.

Anderson, J. L., et al. (2004), The new GFDL global atmosphere and land model AM2-LM2: Evaluation with prescribed SST simulations, *J. Clim.*, *17*, 4641–4673.

Bechtold, P., S. K. Krueger, W. S. Lewellen, E. van Meijgaard, C. H. Moeng, D. A. Randall, A. van Ulden, and S. Wang (1996), Modeling a stratocumulus-topped PBL: Intercomparison among different one-dimensional codes and with large eddy simulation, *Bull. Am. Meteorol. Soc.*, *77*, 2033–2042.

Bretherton, C. S., and M. C. Wyant (1997), Moisture transport, lower-tropospheric stability, and decoupling of cloud-topped boundary layers, *J. Atmos. Sci.*, *54*, 148–167.

Bretherton, C. S., J. R. McCaa, and H. Grenier (2004a), A new parameterization for shallow cumulus convection and its application to marine subtropical cloud-topped boundary layers. Part I: Description and 1-D results, *Mon. Weather Rev.*, *132*, 864–882.

Bretherton, C. S., T. Uttal, C. W. Fairall, S. Yuter, R. Weller, D. Baumgardner, K. Comstock, R. Wood, and G. Raga (2004b), The EPIC 2001 stratocumulus study, *Bull. Am. Meteorol. Soc.*, *85*, 967–977.

Bretherton, C. S., P. N. Blossey, and J. Uchida (2006), Cloud droplet sedimentation, entrainment efficiency, and subtropical stratocumulus albedo, *Geophys. Res. Lett.*, *34*, L17810, doi:10.1029/2006GL026672.

Chen, C., and W. R. Cotton (1987), The physics of the marine stratocumulus-capped mixed layer, *J. Atmos. Sci.*, *44*, 2951–2977.

Chlond, A., F. Müller, and I. Sednev (2004), Numerical simulation of the diurnal cycle of marine stratocumulus during FIRE—A LES and SCM modeling study, *Q. J. R. Meteorol. Soc.*, *130*, 3297–3321.

Collins, W. D., P. J. Rasch, B. A. Boville, J. J. Hack, J. R. McCaa, D. L. Williamson, B. P. Briegleb, C. M. Bitz, S.-J. Lin, and M. Zhang (2006), The formulation and atmospheric simulation of the Community Atmosphere Model version 3 (CAM3), *J. Clim.*, *19*, 2144–2161.

Comstock, K. K., R. Wood, S. E. Yuter, and C. S. Bretherton (2004), Reflectivity and rain rate in and below drizzling stratocumulus, *Q. J. R. Meteorol. Soc.*, *130*, 2891–2918.

Comstock, K. K., C. S. Bretherton, and S. E. Yuter (2005), Mesoscale variability and drizzle in Southeast Pacific stratocumulus, *J. Atmos. Sci.*, *62*, 3792–3807.

De Roode, S. R. (2007), The role of eddy diffusivity profiles on stratocumulus liquid water path biases, *Mon. Weather Rev.*, *135*, 2786–2793.

Duynkerke, P., et al. (2004), Observations and numerical simulations of the diurnal cycle of the EUROCS stratocumulus case, *Q. J. R. Meteorol. Soc.*, *130*, 3269–3296.

Faloona, I., D. H. Lenschow, T. Campos, B. Stevens, M. van Zanten, B. Blomquist, D. Thornton, A. Bandy, and H. Gerber (2005), Observations of entrainment in eastern Pacific marine stratocumulus using three conserved scalars, *J. Atmos. Sci.*, *62*, 3268–3285.

Golaz, J.-C., V. E. Larson, and W. R. Cotton (2002), A pdf-based model for boundary layer clouds. Part I: Method and model description, *J. Atmos. Sci.*, *59*, 3540–3551.

Holtslag, A. A. M., and B. A. Boville (1993), Local versus nonlocal boundary layer diffusion in a global climate model, *J. Clim.*, *6*, 1825–1842.

Khairoutdinov, M., and Y. Kogan (2000), A new cloud physics parameterization in a large-eddy simulation model of marine stratocumulus, *Mon. Weather Rev.*, *128*, 229–243.

Kirkpatrick, M. P., A. S. Ackerman, D. E. Stevens, and N. N. Mansour (2006), On the application of the dynamic Smagorinsky model to large-eddy simulations of the cloud-topped atmospheric boundary layer, *J. Atmos. Sci.*, *64*, 526–546, doi:10.1175/JAS3651.1.

Kitagawa, H., K. Tamiya, S. Murai, M. Nakagawa, T. Komori, K. Yamada, M. Hirai, K. Iwamura, and T. Sakashita (2007), Outline of the operational numerical weather prediction at the Japan Meteorological Agency, Jpn. Meteorol. Agency, Tokyo, Japan.

Klein, S. A., and D. L. Hartmann (1993), The seasonal cycle of low stratiform clouds, *J. Clim.*, *6*, 1587–1606.

Larson, V. E., and J.-C. Golaz (2005), Using probability density functions to derive consistent closure relationships among higher-order moments, *Mon. Weather Rev.*, *133*, 1023–1042.

Larson, V. E., K. E. Kotenberg, and N. B. Wood (2007), An analytic longwave radiation formula for liquid layer clouds, *Mon. Weather Rev.*, *135*, 689–699.

Lenderink, G., B. J. J. M. van den Hurk, E. van Meijgaard, A. P. van Ulden, and J. W. M. Cuijpers (2003), Simulation of present-day climate in RACMO2: First results and model developments, *KNMI-TR 252*, 24 pp., Koninklijk Nederlands Meteorol. Inst., De Bilt, Netherlands.

Lock, A. P., A. R. Brown, M. R. Bush, G. M. Martin, and R. N. B. Smith (2000), A new boundary layer mixing scheme. Part I: Scheme description and single-column model tests, *Mon. Weather Rev.*, *128*, 3187–3199.

Martin, G. M., M. A. Ringer, V. D. Pope, A. Jones, C. Dearden, and T. J. Hinton (2006), The physical properties of the atmosphere in the new Hadley Centre Global Environmental Model, HadGEM1. Part 1: Model description and global climatology, *J. Clim.*, *19*, 1274–1301.

Moeng, C.-H., et al. (1996), Simulation of a stratocumulus-topped planetary boundary layer: Intercomparison among different numerical codes, *Bull. Am. Meteorol. Soc.*, *77*, 261–278.

Roeckner, E., K. Arpe, L. Bengtsson, M. Christoph, M. Claussen, L. Dümenil, M. Esch, M. Giorgetta, U. Schlese, and U. Schulzweida (1996), The atmospheric general circulation model ECHAM4: Model description and simulation of present day climate, *Rep. 218,* Max-Planck-Inst. für Meteorol., Hamburg, Germany.

Roeckner, E., et al. (2003),The atmospheric general circulation model ECHAM 5. Part I: Model description, *Rep. 349,* Max-Planck-Inst. für Meteorol., Hamburg, Germany.

Rotstayn, L. D. (1997), A physically based scheme for the treatment of stratiform clouds and precipitation in large-scale models. I: Description and evaluation of the microphysical processes, *Q. J. R. Meteorol. Soc.*, *123*, 1227–1282.

Savic-Jovcic, V., and B. Stevens (2007), The structure and mesoscale organization of precipitating stratocumulus, *J. Atmos. Sci*, in press.

Smith, R. N. B. (1990), A scheme for predicting layer clouds and their water content in a general circulation model, *Q. J. R. Meteorol. Soc.*, *116*, 435–460.

Stevens, B., et al. (2003), Dynamics and chemistry of marine stratocumulus-DYCOMS-II, *Bull. Am. Meteorol. Soc.*, *84*, 579–593.

Stevens, B., et al. (2005), Evaluation of large-eddy simulations via observations of nocturnal marine stratocumulus, *Mon. Weather Rev.*, *133*, 1443–1462.

Stevens, D. E., A. S. Ackerman, and C. S. Bretherton (2002), Effect of domain size and numerical resolution on the simulation of shallow cumulus convection, *J. Atmos. Sci.*, *59*, 3285–3301.

Sundqvist, H. (1978), A parameterization scheme for non-convective condensation including prediction of cloud water content, *Q. J. R. Meteorol. Soc.*, *104*, 677–690.

Sundqvist, H., E. Berge, and J. E. Kristjansson (1989), Condensation and cloud parameterization studies with a mesoscale numerical weather prediction model, *Mon. Weather Rev.*, *117*, 1641–1657.

Tiedtke, M. (1993), Representation of clouds in large-scale models, *Mon. Weather Rev.*, *121*, 3040–3061.

Tripoli, G. J., and W. R. Cotton (1980), A numerical investigation of several factors contributing to the observed variable intensity of deep convection over south Florida, *J. Appl. Meteorol.*, *19*, 1037–1063.

Turton, J., and S. Nicholls (1987), A study of the diurnal variation of stratocumulus using a multiple mixed layer model, *Q. J. R. Meteorol. Soc.*, *113*(477), 969–1009.

vanZanten, M. C., and B. Stevens (2005), Observations of the structure of heavily precipitating marine stratocumulus, *J. Atmos. Sci.*, *62*, 4327–4342.

vanZanten, M. C., B. Stevens, G. Vali, and D. H. Lenschow (2005), Observations of drizzle in nocturnal marine stratocumulus, *J. Atmos. Sci.*, *62*, 88–106.

Wilson, D. R., and S. P. Ballard (1999), A microphysically based precipitation scheme for the UK Meterological Office Unified Model, *Q. J. R. Meteorol. Soc.*, *125*, 1607–1636.

Zhu, P., et al. (2005), Intercomparison and interpretation of single-column model simulations of a nocturnal stratocumulus-topped marine boundary layer, *Mon. Weather Rev.*, *133*, 2741–2758.

A. S. Ackerman, NASA Goddard Institute for Space Studies, New York, NY 10025, USA.

C. S. Bretherton, S. Park, and M. C. Wyant, Department of Atmospheric Sciences, Box 351640, University of Washington, Seattle, WA 98195, USA. (mwyant@atmos.washington.edu)

A. Chlond, Max Planck Institute for Meteorology, D-20146 Hamburg, Germany.

S. R. de Roode, Koninklijk Nederlands Meteorologisch Instituut, NL-3730 AE De Bilt, Netherlands.

B. M. Griffin and V. E. Larson, Department of Mathematical Sciences, University of Wisconsin-Milwaukee, Milwaukee, WI 53201, USA.

H. Kitagawa, Japan Meteorological Agency, Tokyo 100-8122, Japan.

C.-L. Lappen, Department of Atmospheric Science, Colorado State University, Fort Collins, CO 80523, USA.

A. Lock, Met Office, Exeter EX1 3PB, UK.

J. Uchida, Department of Applied Mathematics, University of Washington, Seattle, WA 98195, USA.

M. Zhao, NOAA Geophysical Fluid Dynamics Laboratory, Princeton, NJ 08540, USA.